

Topological slow light and rainbow trapping of surface wave in valley photonic crystal bounded by air

Shuheng Chen(陈书恒), Yi Qi(齐奕), Yucen Li(李昱岑), Qihao Wang(王琪皓), and Yuanjiang Xiang(项元江)

Citation:. Phys. B, 2024, 33 (**11**): 118701. DOI: 10.1088/1674-1056/ad7fd2
Journal homepage: http://cpb.iphy.ac.cn; http://iopscience.iop.org/cpb

What follows is a list of articles you may be interested in

Influence of viscous force on the dynamic process of micro-sphere in optical tweezers

Jing Liu(刘静), Xingyu Wu(吴星宇), Yimin Feng(冯怡敏), Mian Zheng(郑冕), and Zhiyuan Li(李志远)
Chin. Phys. B, 2023, 32 (**10**): 108704. DOI: 10.1088/1674-1056/acddd1

Transverse manipulation of particles using Bessel beam of tunable size generated by cross-phase modulation

Xiang-Lai Qiao(乔响来), Xue-Mei Cheng(程雪梅), Qian Zhang(张倩), Wen-Ding Zhang(张文定), Zhao-Yu Ren(任兆玉), and Jin-Tao Bai(白晋涛)
Chin. Phys. B, 2023, 32 (**4**): 048703. DOI: 10.1088/1674-1056/ac8925

Chiral lateral optical force near plasmonic ring induced by Laguerre-Gaussian beam

Ying-Dong Nie(聂英东), Zhi-Guang Sun(孙智广), and Yu-Rui Fang(方蔚瑞)
Chin. Phys. B, 2023, 32 (**1**): 018702. DOI: 10.1088/1674-1056/ac6eea

Excessive levitation for the efficient loading of large-volume optical dipole traps

Xiaoqing Wang(王晓青), Yuqing Li(李玉清), Guosheng Feng(冯国胜), Jizhou Wu(武寄洲), Jie Ma(马杰), Liantuan Xiao(肖连团), Suotang Jia(贾锁堂)
Chin. Phys. B, 2018, 27 (**1**): 018702. DOI: 10.1088/1674-1056/27/1/018702

Microtrap on a concave grating reflector for atom trapping

Hui Zhang(张 慧), Tao Li(李涛), Ya-Ling Yin(尹亚玲), Xing-Jia Li(李兴佳), Yong Xia(夏 勇), Jian-Ping Yin(印建平)
Chin. Phys. B, 2016, 25 (**8**): 087802. DOI: 10.1088/1674-1056/25/8/087802

Topological slow light and rainbow trapping of surface wave in valley photonic crystal bounded by air

Shuheng Chen(陈书恒)[1,2], Yi Qi(齐奕)[1,2], Yucen Li(李昱岑)[1,2], Qihao Wang(王琪皓)[1,2], and Yuanjiang Xiang(项元江)[1,2,†]

[1] *Research Institute of Hunan University in Chongqing, Chongqing* 401120, *China*
[2] *School of Physics and Electronics, Hunan University, Changsha* 410082, *China*

(Received 28 August 2024; revised manuscript received 23 September 2024; accepted manuscript online 26 September 2024)

Topological slow light and rainbow trapping tend to rely on large-scale interface structure in previous research work, which have restricted further miniaturization. In this work, we propose a method to realize slow light and rainbow trapping at the zigzag edge of a single valley photonic crystals (VPCs) bounded by air, which is very different from previous studies where rainbow trapping is supported at the interface separating two VPCs with inversion symmetry. By constructing the VPC–air boundaries and VPC–VPC interfaces experimentally, we have observed the topologically protected rainbow trapping simultaneously at the external and internal boundary. This work provides a feasible platform for the miniaturized optical communication devices such as optical buffers, optical storage and optical routing.

Keywords: topological slow light, rainbow trapping, valley photonic crystals

PACS: 87.80.Cc, 03.65.Vf, 42.70.Qs **DOI:** 10.1088/1674-1056/ad7fd2

1. Introduction

Topological photonic crystals (PCs) attract enormous attention because of their potential to realize advanced optical systems, which are immune to certain disorders and backscattering.[1–5] In general, a graphene-like PC possesses a pair of degenerate but nonequivalent energy extreme in momentum space, named valley, which are guaranteed by the lattices spatial symmetry. By breaking the spatial symmetry of the lattice, the degeneracy would lift up, forming a nontrivial bandgap. Valley edge states (VESs) can be realized at the interface between two topological photonic crystals with different Chern number.[6–8] Chiral edge states (CESs) are existed at the external boundary of the VPC. The transmissions of CESs require no domain wall and thus reduce the size of VPC, greatly enhancing the miniaturization development of VPC.[9–13]

The slow light effect can be explained as the group velocity of the light reduce greatly and thus enhance the interaction between matter and light and control the flow of light. What's more, slow light has been widely applied in optical storage, optical switching and nonlinear optics with broad prospects. Rainbow trapping is defined as the light of different frequencies are spatially separated and trapped at different positions, provides a feasible technique of the frequency routing of slow light.[14–27] Recently researchers have proposed a series of methods to realize slow rainbow trapping, for example, building a gradient changing interface by contracting and expanding the lattice of two-dimensional (2D) dielectric topological PCs.[28] However, the domain-free rainbow trapping has not been realized, and it is still a challenge to verify the relevant experiments, which has restricted the miniaturization of optical devices.

In this paper, we use a VPC which can simultaneously realize topological slow light and rainbow trapping at the VPC–air boundary and VPC–VPC interface. Thanks to the bulk-boundary correspondence, nontrivial VPC and air interface will exist topological protected CES, two types of VPCs' interface will exist topological protected VES. Therefore, we precisely design a gradient changing structure at three interfaces by gradually adjusting the translational parameters of deformation domain along the y direction. This work is beneficial to further miniaturization and functionalization of photonic integrated circuits and dramatically promotes the application of topological photonic states in optic devices.

2. Structure design and dispersion analysis

As shown in Fig. 1(a), the VPC is embedded in the air background, composed of dielectric rods. The lattice vectors are represented by $\boldsymbol{a}_1$ and $\boldsymbol{a}_2$ with the same lattice constant $a = 6\sqrt{3}$ mm. The unit cell consists of two types of rods, marked by a black hexagon. Their diameters are devoted by d_A and d_B, respectively. A rod has a diameter of $d_A = 5$ mm, while B rod has a diameter of $d_B = 3$ mm. The refractive index of the rods is $n_{rod} = 3.13$. The finite element method is used to calculate the topological behavior of VPC. As shown in Fig. 1(c), when $d_A = d_B = 4$ mm, the band degeneracy

†Corresponding author. E-mail: xiangyuanjiang@126.com

© 2024 Chinese Physical Society and IOP Publishing Ltd

occurs at K point of Brillouin zone (BZ). The Dirac points (marked by red dots) are formed at K point in band 1 and band 2, and band 5. When the symmetry of the unit cell is broken by setting $d_A \neq d_B$, the degeneracy at two equal K points is lifted, two complete band gaps will appear in the whole Brillouin zone, as shown in the blue region in Fig. 1(d). We define the VPC with $d_A = 5$ mm, $d_B = 3$ mm as VPC1 and define the VPC with $d_A = 3$ mm, $d_B = 5$ mm as VPC2. By calculating the band structure of VPC1 and VPC2, we can find that there are two valley band gaps of 8.74 GHz and 18.52 GHz. Although the band structure of the VPC1 and VPC2 are the same, their topological properties are different. This can be described using valley Chern numbers and circularly polarized phase vortex. As shown in Figs. 1(b) and 1(e), taking the first band as an example, the valley Chern number at the K valley of VPC1 can be characterized by left-handed circular polarization (LCP), while the valley Chern number at the K valley of VPC2 can be characterized by right-handed circular polarization (RCP). For the same type of VPC, the phase changes at the K and K' valleys are opposite. Thus, a topological phase transition occurs at the K and K' valleys when the VPC transitions from VPC2 to VPC1. According to time-reversal symmetry, the K valley of VPC1 is equivalent to the K' valley of VPC2, and the K valley of VPC2 is equivalent to the K' valley of VPC1. As Δd changes from -2 mm to 0 and then to 2 mm, the band structure undergoes a process of opening, closing, and reopening, accompanied by a reversal of the direction of the valley Chern numbers, indicating the occurrence of a valley topological phase transition during this process.

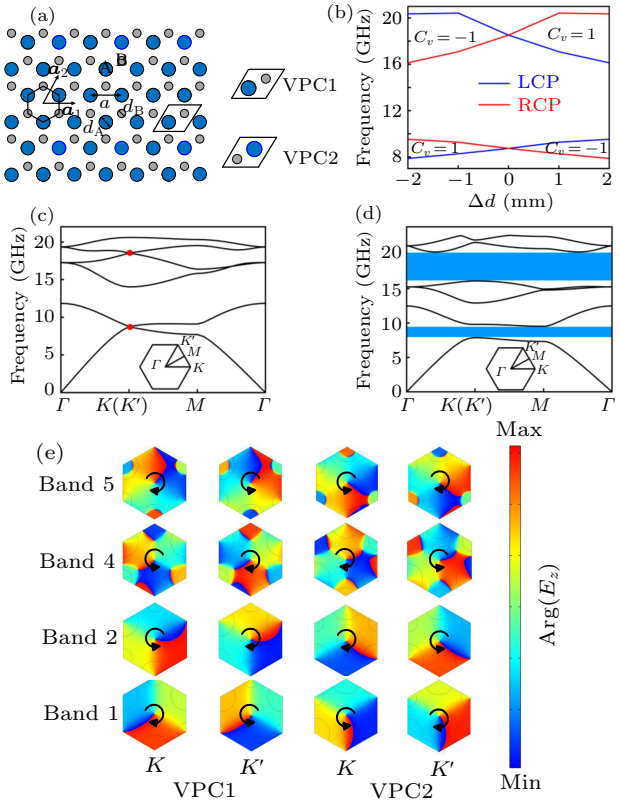


Fig. 1. (a) Schematic diagram of 2D valley photonic crystal composed of two Al_2O_3 rods of different diameters which are in a background air. (b) Relationship between topological phase transition at the K valley and variation of Δd. (c) Band structure at $\Delta d = 0$, with the inset showing the first Brillouin zone where the red dots indicate the degenerate Dirac points. (d) Band structure at $\Delta d = 2$ mm, with the inset showing the first Brillouin zone where the light blue rectangle represents the bandgap of the valley photonic crystal. (e) Phase distribution of the 1st, 2nd, 4th, and 5th bands at the K and K' points for VPC1 and VPC2, where the clockwise arrows represent right circularly polarized (RCP) orbital angular momentum, and the counterclockwise arrows represent left circularly polarized (LCP) orbital angular momentum.

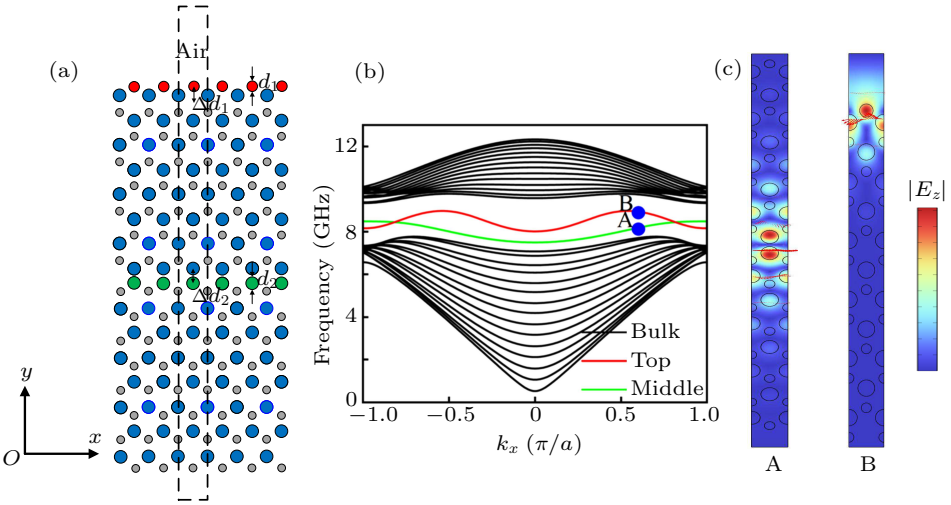


Fig. 2. (a) Schematic diagram of supercell structure. (b) Dispersion curves of the valley edge state and chiral edge states. (c) The electric field distribution of $|E_z|$ and poynting vectors distribution at points A, B with red arrows indicating the direction of energy flow.

The nonzero valley-Chern number implies that the VPC can support nontrivial edge states. According to the bulk-edge correspondence, topological edge exist at the interface of two systems with different Chern numbers. Here we build a VPC composed of VPC1 and VPC2 with opposite valley Chern numbers, where the top boundary rods are used to tune the dispersion of the topological states, the diameter of top boundary rod is $d_1 = 4$ mm as shown in Fig. 2(a). Similarly nontrivial VPC1 and air (can be considered to have $C_v = 0$) can form two sets of topological edge states. Figure 2(b)

shows the VESs and CESs of the proposed VPC in Fig. 2(a), where black, green, and red curves represent the bulk state, the CESs formed by the contact of VPC1 with air and the VESs generated by the contact of VPC1 with VPC2, respectively. As shown in Figs. 2(a) and 2(b), we choose B ($0.6\pi/a$, 8.916 GHz) and from the electric field distribution, it can be seen that the electric field is well localized near the boundary between the valley PCs and air. It can be seen from the Poynting vectors that points B have negative group velocities and the energy flow directions point to the negative x axis. Then, we choose A ($0.6\pi/a$, 8.187 GHz), and it can be seen from the electric field distribution that the electric field is well localized near the boundary of the two photonic crystal structures. It can be seen from the Poynting vector that point A has a positive group velocity and its energy flow direction points to the x axis positive direction.

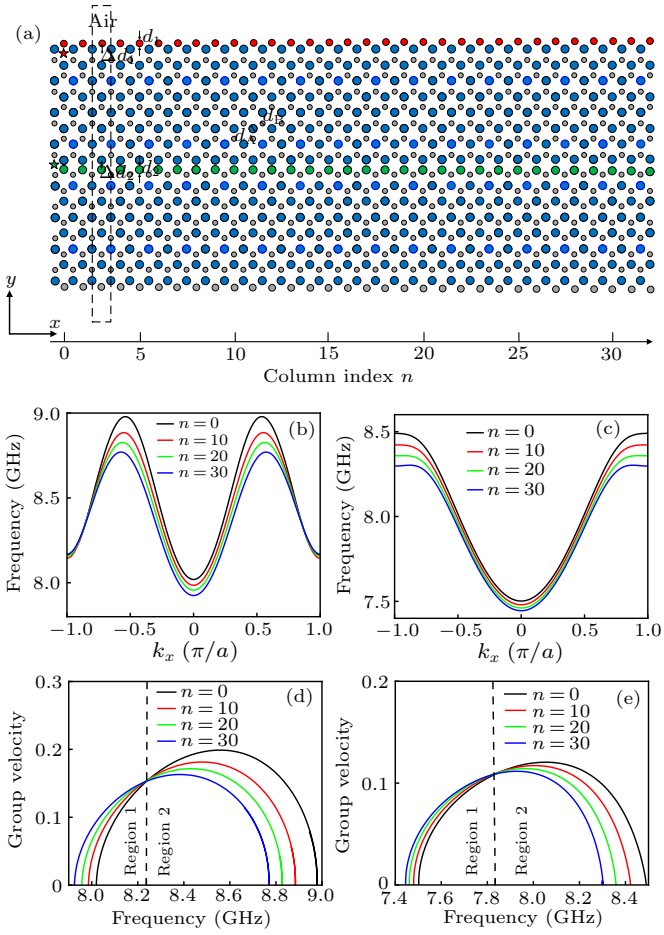


Fig. 3. (a) Schematic diagram of topological rainbow trapping. (b) Chiral edge state generated by VPC1 in contact with air. (c) Valley edge state generated by VPC1 in contact with VPC2. (d) Group velocities corresponding to chiral edge states generated by VPC1 in contact with air. (e) Group velocities corresponding to valley edge states generated by VPC1 in contact with VPC2.

Figure 3(a) shows the schematic diagram of topological rainbow trapping made of alumina material with the refractive index of 3.13, the distance from the center of the upper red cylinder to the center of the positive hexagon is Δd_1, the distance from the center of the middle blue cylinder to the center of the green cylinder is Δd_2. Based on the method of rainbow trapping by introducing gradient changes into the structure,[20] we introduced gradient variations into the structure, at the leftmost side ($n = 0$) along the positive x direction, $\Delta d_1 = \Delta d_2 = a/\sqrt{3}$, the green cylinders in the middle channel move $0.002a$ towards the negative y direction each time; meanwhile, the red cylinders at the top move $0.002a$ towards the positive y direction each time, in other words, $\Delta d_1 = \Delta d_2 = a/\sqrt{3} + 0.002a \cdot n$. Figures 3(b)–3(e) show the dispersion relations and group velocities for the VESs and the CESs at the air boundary, and we find that by introducing a gradient changes at the top and middle boundary of the VPC, these boundary states gradually move downward and the group velocities gradually move to lower frequencies as n increases. For a fixed frequency, the electromagnetic wave undergoes different states, which leads to a decrease in the group velocity along the propagation direction until the electromagnetic wave is no longer allowed to propagate. Therefore, this property provides a viable method for spatially separating boundary states of different frequencies and realizing topological rainbow trapping.

2.1. Sample preparation and experimental verification

In this experiment, we choose Al_2O_3 dielectric columns with different diameters of 3 mm, 4 mm, and 5 mm and a height of 10 mm to construct composite structures for study. During the construction of the experimental model, we use a pluggable self-assembled template to fix the experimental materials. In the first set of experiments, we prepared a 30-layer three-channel VPCs waveguide with gradient variations and input signals from the three channels respectively, as shown in Figs. 4(a) and 4(d), and the positions of excitation probes were marked with red and green, respectively, and the rainbow trapping effect of the top channel and the middle channel are observed by computer. Figures 4(b), 4(c) and 4(e), 4(f) show the electric field distribution of numerical simulation and experimental measurement, respectively, we find that the frequency bands of the middle channel gradually shorten the propagation distance with the increase of frequency, corresponding the region 2 in Fig. 3(d). While the top channel shows the opposite trend, the propagation distance gradually increases with the increase of frequency, corresponding the region 2 in Fig. 3(c). These phenomena are clearly demonstrated in the microwave experiments. Due to the difference in relative permittivity between the materials used in the simulation and those used in the experiment, and there is an air layer of certain thickness between the receiving probe and the sample surface. This results in a reduced effective refractive index, causing the frequency range of the rainbow trapping effect observed in the experiment to shift upward by approximately 1 GHz–2 GHz. However, it remains within the first bandgap of the VPCs. The pattern of the rainbow trapping effect observed in the experiment is consistent with the simulation.

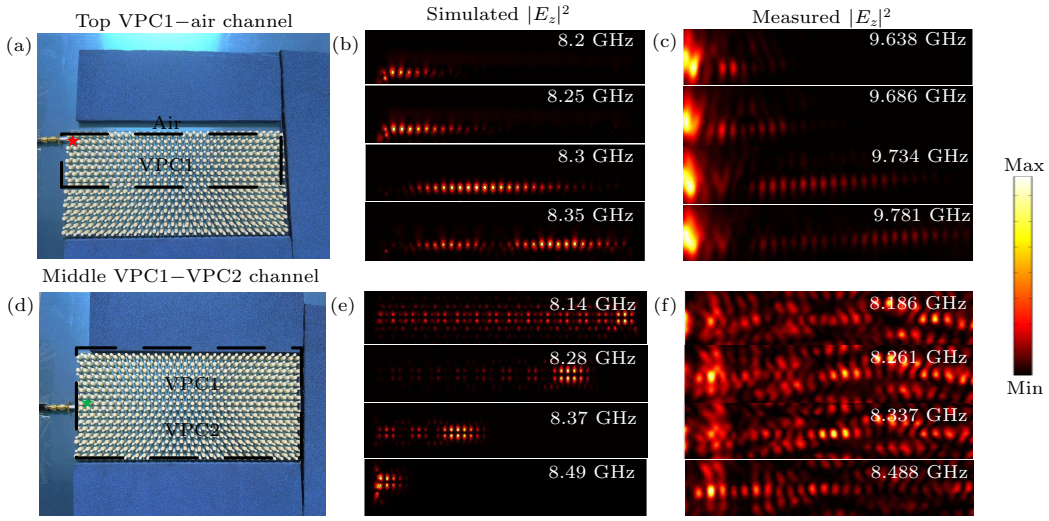


Fig. 4. (a) Experimental setup for the sample with an excitation probe of top VPC1–air channel. (b) Simulated electric field distribution top VPC1–air channel. (c) Measured electric field distribution using microwave near-field characterization in the top VPC1–air channel. (d) Experimental setup for the sample with an excitation probe in the middle VPC1–VPC2 channel. (e) Simulated electric field distribution in the middle VPC1–VPC2 channel. (f) Measured electric field distribution using microwave near-field characterization in the middle VPC1–VPC2 channel.

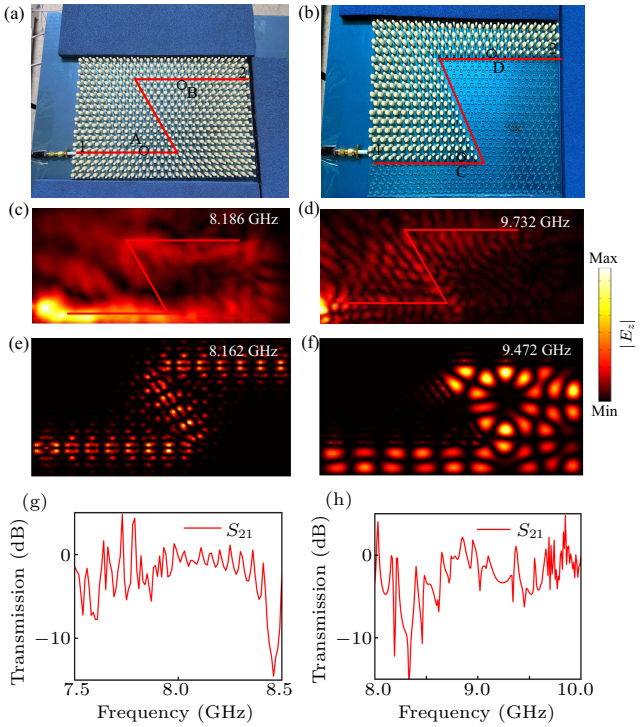


Fig. 5. (a) Zigzag waveguide samples at the valley edge and their excitation settings. (b) Zigzag waveguide samples at the air edge and their excitation settings. (c) Electric field distribution of the zigzag waveguide at the valley edge with defect (measured). (d) Electric field distribution of the zigzag waveguide at the air edge with defect (measured). (e) Electric field distribution of the zigzag waveguide at the valley edge without defect (simulated). (f) Electric field distribution of the zigzag waveguide at the air edge without defect (simulated). (g) Transmission characteristics of the valley edge without defects. (h) Transmission characteristics of the air edge without defects.

In order to further verify the unidirectionality and robustness of the designed VPCs waveguide, in the second set of experiments we perform surface electric field scans on the valley-boundary and air-boundary zigzag waveguides, as shown in Figs. 5(a) and 5(b). Firstly, we measure the zigzag waveguide at the valley boundary and introduce defects at points A and B. When the signal source is input from one end, we can clearly observe the electromagnetic wave with a frequency of 8.186 GHz traveling along the zigzag pattern from Fig. 5(c). Secondly, we remove some of the cylinders and replace the 5 mm diameter cylinders at the boundary with 4 mm diameter cylinders so that the Z-channel forms an air boundary and defects are introduced at points C and D. We put the signal source from one end and observe the image of the electric field distribution. From Fig. 5(d), it can be seen that the electromagnetic wave with a frequency of 9.732 GHz can still be transmitted normally along the Z shape of the air boundary. In addition, we used numerical simulation to analyze the transmission characteristics of the zigzag waveguide when there are no defects on the upper boundary and valley boundary. From Figs. 5(e)–5(h), it can be seen that both the large turning angle and the modeled perturbation fully demonstrate the extreme unidirectionality and robustness of our designed VPCs waveguide.

3. Conclusion and perspectives

In conclusion, according to the problem of topological rainbow trapping relying on large scale domain walls, we propose a method to realize slow light rainbow trapping simultaneously at the external and internal boundary of a VPC, which is created by gradually increasing the structure parameter. By carring out numerical simulations and microwave near-field characterization of rainbow trapping, unidirectionality of the edge state and robustness, we successfully verifies the reasonableness and feasibility of the designed structure, which provides a new scheme for the realization of highly integrated and miniaturized photonic devices, multifrequency routing, and

wavelength-division multiplexing.

Acknowledgements

Project supported by the National Natural Science Foundation of China (Grant No. 12374302) and the Natural Science Foundation of Chongqing (Grant No. CSTB2022NSCQ-MSX0872).

References

[1] Wang Z, Chong Y D, Joannopoulos J D and Soljačić M 2009 *Nature* **461** 772
[2] Haldane F D and Raghu S 2008 *Phys. Rev. Lett.* **100** 013904
[3] Baba T 2008 *Nat. Photon.* **2** 465
[4] Haldane F D 1988 *Phys. Rev. Lett.* **61** 2015
[5] Hatsugai Y 1993 *Phys. Rev. Lett.* **71** 3697
[6] Dong J W, Chen X D, Zhu H, Wang Y and Zhang X 2017 *Nat. Mater.* **16** 298
[7] Ma T and Shvets G 2016 *New J. Phys.* **18** 025012
[8] Chen X D, Zhao F L, Chen M and Dong J W 2017 *Phys. Rev. B* **96** 020202
[9] Chen M, Jiang L J, Lan Z and Sha W 2020 *Opt. Express* **28** 14428
[10] Feng Y, Zhang Z, Qin F, Lan Z, Sha W and Xu Y 2022 *Opt. Lett.* **47** 3107
[11] Wei G, Liu Z, Wu H, Wang L, Wang S and Xiao J 2022 *Opt. Lett.* **47** 3007
[12] Zhang Z, Lan Z, Xie Y, Chen M, Sha W and Xu Y 2021 *Phys. Rev. Lett.* **16** 064036
[13] Yu L, Xue H and Zhang B 2021 *Appl. Phys. Lett.* **118** 071102
[14] Wu L H and Hu X 2015 *Phys. Rev. Lett.* **114** 223901
[15] Elshahat S, Wang C, Zhang H and Lu C 2021 *Appl. Phys. Lett.* **119** 230505
[16] Chen J, Qin Q, Peng C, Liang W and Li Z Y 2021 *Front. Mater.* **8** 728991
[17] Lu C, Wang C, Xiao M, Zhang Z Q and Chan C T 2021 *Phys. Rev. Lett.* **126** 113902
[18] Lu C, Sun Y, Wang C, Zhang H, Zhao W, Hu X, Xiao M, Ding W, Liu Y C and Chan C T 2022 *Nat. Commun.* **13** 2586
[19] Zhao W, Zheng Y and Lu C 2022 *Photon. Res.* **10** 2728
[20] Mao Y, Li Z, Hu W, Dai X and Xiang Y 2022 *J. Lightwave Technol.* **40** 5152
[21] Liang L, Zhou X, Hu J H, Wang H X, Jiang J H and Hou B 2022 *Opt. Lett.* **47** 1454
[22] Liu J, Lu X, Dai X and Xiang Y 2022 *J. Appl. Phys.* **132** 173105
[23] Neseli B, Bor E, Kurt H and Turduev M 2020 *J. Opt. Soc. Am. B* **37** 1249
[24] Ding F, Mao Y, Shen J, Dai X and Xiang Y 2022 *Opt. Lett.* **47** 5650
[25] Mao Y, Hu W, Li Z, Dai X and Xiang Y 2022 *J. Opt. Soc. Am. B* **39** 1241
[26] Shen Y F, Xu X, Sun M, Zhou W J and Chang Y J 2024 *Chin. Phys. B* **33** 044203
[27] Wan X, Peng C, Li G, Yang J and Qi X 2023 *Chin. Phys. B* **32** 114208
[28] Zhang H, Qian L, Wang C, Ji C Y, Liu Y, Chen J and Lu C 2021 *Opt. Lett.* **46** 1237